RESEARCH ARTICLE

Analytical Method for Compensation Choke Geometry Optimization to Minimize Losses

VLADIMIR KINDL[1], (Member, IEEE), BOHUMIL SKALA[1],
AND MICHAL FRIVALDSKY[ID][2], (Member, IEEE)

[1]Department of Power Electronics and Machines, Faculty of Electrical Engineering, University of West Bohemia, 306 14 Pilsen, Czech Republic
[2]Department of Electronics and Mechatronics, Faculty of Electrical Engineering and Information Technologies, University of Žilina, 010 26 Žilina, Slovakia

Corresponding author: Michal Frivaldsky (michal.frivaldsky@feit.uniza.sk)

ABSTRACT The article presents an analytical method for optimizing the geometry of the magnetic core of a three-phase compensation choke. The method describes the process of identification the fringing magnetic fields and the corresponding magnetic reluctances of the magnetic core, the flux density calculation even in the case of the core supersaturation and the total losses estimation. It shows finding the trade-off between the size/weight of the inductor and the magnetic core with respect to the overall losses and demonstrates their minimization. The mathematical model for the flux's identification is based on a standard iterative calculation using the analogy to electrical circuits but includes a new approach to the calculation of fringing magnetic fields caused by the air gapped magnetic core. The presented method is verified by the finite element method (FEM) using the engineering calculation software ANSYS.

INDEX TERMS Compensation choke, coil, magnetic field, flux density, reluctance, power losses.

I. INTRODUCTION

The continual technological improvements in the area of power electronic systems (electrical vehicles, energy storage systems, renewable energy, energy distribution, consumer electronic, lightning systems and more electric aircraft) drives development to a much higher desire for improvements of the system properties like efficiency, robustness and the highest possible power density [1].

In parallel with the development of ''cutting – edge'' technological systems, the demands on the annual global energy consumption are also continuously rising. In this context, it is very important to understand that even small improvement in the energy efficiency and/or in the quality of the electrical supply grid (reactive power compensation), yields to a significant savings [2]. Due to these reasons the development of a wide scope of methods and techniques for power compensation and energy consumption have been realized and verified. One of the most common is the use

of passive compensators of the power using compensation chokes and capacitors. The principles of operation and the design methods of passive power compensator elements are relatively well known and well described in [3], [4], and [5], while in addition to compensating the reactive power, these systems also have the role to prevent the parallel resonance and amplification harmonic current occurring.

The compensation choke is an important component for high-power industrial applications that require reactive power suppression, e.g., metal-clad HV cables, long open-circuit power lines, photovoltaic powerplant, etc. As this component is a common and frequently used by the industry (millions are sold each year), any increase in its efficiency means significant savings in a global electricity consumption and can thus contribute to meeting the EU's commitments, which have adopted very ambitious targets to reduce net greenhouse gas emissions by a further 55% by 2030 compared to 1990 levels [6], [7], [8].

Inductive components, their design and analysis have been the subject of research during the development of various power and industrial application. Literature provides

The associate editor coordinating the review of this manuscript and approving it for publication was Chandan Kumar[ID].

numerous procedures to design the inductive components and analyze their losses and power efficiency. The power losses are usually classified into two groups: the iron core losses and the I²R losses [9], [10], [11], [12], [13]. As the iron core losses are caused by the eddy currents induced in the core and by the magnetic agitation of the molecules in the core and their resistance to being moved during alternating magnetization, the I²R losses are caused by the winding currents producing Joule heat. The research provided within [14], [15], [16], [17], [18] is based mostly on the use of the relations of power losses to the frequency of operation, magnetic flux density and empirically expressed constants dependent on the component geometry. As the proposed approaches provide indicative values for the initial design, they do not allow to analyze the magnetic circuit of the inductor, so the power loss estimation may not be directly related to the phenomena dealing with magnetic leakage field and fringing flux [19], [20], [21].

This paper presents a procedure for optimizing the initial electromagnetic design of a three-phase compensating choke reflecting the optimal ratio between losses produced in the iron core and the windings. The optimization method uses the standard analytical model to analyze the magnetic core improved with a detailed calculation of fringing magnetic fields using an iterative calculation working even when the magnetic circuit is oversaturated. The proposed method is demonstrated using a case study and verified by the finite element analyses (FEA).

II. CORE SHAPE AND WINDING LOSSES
Although the literature contains basic analytical design procedures for choke cores [22], [23], [24], [25], [26], [27], it is not always possible to find the power losses optimization in a particular geometry including the leakage and the fringing magnetic fluxes [23]. The proposed methodology is following with the next stpes. We start with defining the choke core topology (Figure 1) described by independent dimensions a and b. The aim is to find the optimal ratio between them leading to the winding losses minimization.
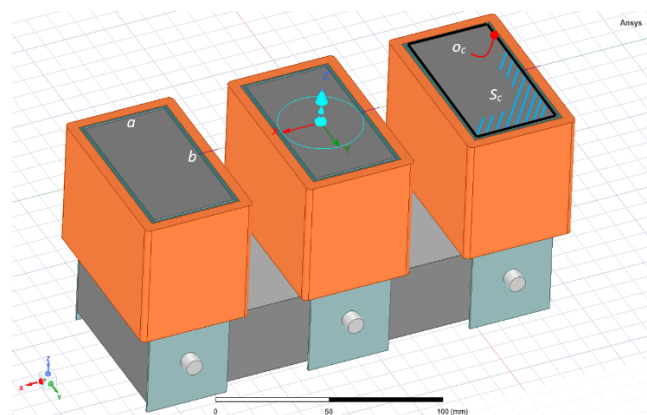

FIGURE 1. Example of assembly of three phase compensation choke.

For one turn of the coil with perimeter o_c and the cross-section area S_c, we write (1).

$$S_c = ab$$
$$o_c = 2(a + b) \tag{1}$$

Combining (1) gives (2).

$$o_c = 2\left(a + \frac{S_c}{a}\right) \tag{2}$$

Minimal o_c is then found using the first derivative as indicated in (3)

$$d\frac{o_c}{da} = 0; \implies 2\left(\frac{a^2 + S_c}{a}\right) = 0 \implies a = \sqrt{S_c} \tag{3}$$

By inserting (3) back into (1) we get (4), which shows that the square cross-section of the magnetic core leads to the shortest possible coil turns and hence to the minimal I²R losses.

$$a^2 = ab \implies a = b \tag{4}$$

Considering the square shape of the coil, Figure 2 shows the winding composition having square corners to obtain formulas as simple as possible. Conductors of radii r_v are assumed to form tightly wound coils. The conductor insulation extends the distance between two adjacent turns and therefore $\delta \geq 2r_v$. Total number of turns N is distributed within l layers with k turns at one layer. It is also assumed that the last layer may not be completely occupied.
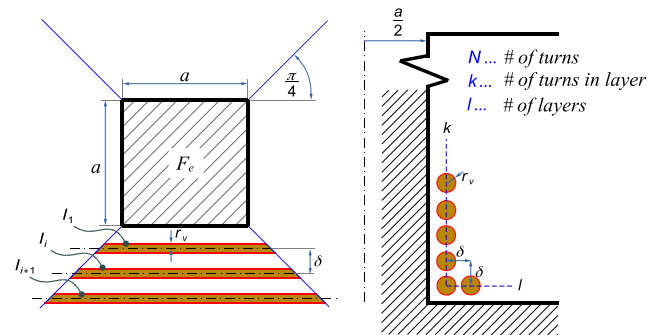

FIGURE 2. Schematic representation of the winding turns.

The length of the i-th quarter of one coil turn is found from equation (5).

$$l_i = a + 2[r_v + \delta(i-1)] \tag{5}$$

The length of all quarter-turns is summed by (6):

$$l_{c4} = \sum_{i=1}^{\frac{N-mod(N,k)}{k}} k[a + 2[r_v + \delta(i-1)]] + mod(N,k)\left[a + 2\left(r_v + \delta\frac{N-mod(N,k)}{k}\right)\right] \tag{6}$$

Substituting (7) back into (6) gives (8), which reflects the total length of turns, i.e., the length of the winding conductor.

$$x = mod(N, k)$$
$$l = \frac{N - mod(N, k)}{k} \qquad (7)$$

Here the symbol $mod(N, k)$ expresses the residue after division, or in other words "modulo" which is the characteristic for integer division. The total length of the conductor is then:

$$l_c = 4\left[2l\delta x + (kl + x)(a + 2r_v) + k\delta l(l - 1)\right] \qquad (8)$$

Thus, the value of the winding resistance can be calculated using (9).

$$R_{DC}(\vartheta) = \rho_{Cu}(\vartheta)\frac{l_c}{\pi r_v^2},$$
$$\rho_{Cu}(\vartheta) = \rho_{Cu}(20°C)\left[1 + \alpha_{Cu}(\vartheta - 20°C)\right] \qquad (9)$$

If condition $r_v \ll \sqrt{\rho_{Cu}/\pi f \mu_0}$ holds, we may consider the resistance as independent of the frequency. When higher operational frequencies are expected, it is recommended to approximate the resistance by (10).

$$R_{AC}(f, \vartheta) = \begin{cases} \rho_{Cu}(\vartheta)\dfrac{l_c}{\pi \delta_{Cu}(\vartheta)(2r_v - \delta_{Cu})}, \\ \qquad \delta_{Cu}(\vartheta) \le r_v \\ \rho_{Cu}(\vartheta)\dfrac{l_c}{\pi r_v^2}\left(1 + \dfrac{1}{48}\left(\dfrac{r_v}{\delta_{Cu}(\vartheta)}\right)^4\right), \\ \qquad \delta_{Cu}(\vartheta) > r_v \end{cases}$$

$$\delta_{Cu}(\vartheta) = \sqrt{\rho_{Cu}(\vartheta)/\pi f \mu_0}$$
$$\rho_{Cu}(\vartheta) = \rho_{Cu}(20°C)\left[1 + \alpha_{Cu}(\vartheta - 20°C)\right] \qquad (10)$$

In this case, mainline frequency will result in the I^{2}R losses according to (11).

$$\Delta P_j(\vartheta) = 3I^2 R_{DC}(\vartheta) \qquad (11)$$

III. ANALYSES OF THE CHOCKE MAGNETIC CIRCUIT

A. THE AIR GAP RELUCTANCES

The magnetic circuit model is based on the system reluctances or permeances description. Fig. 3 shows that an accurate analytical description of either leakage or fringing magnetic fields is a complex task and is therefore reasonable
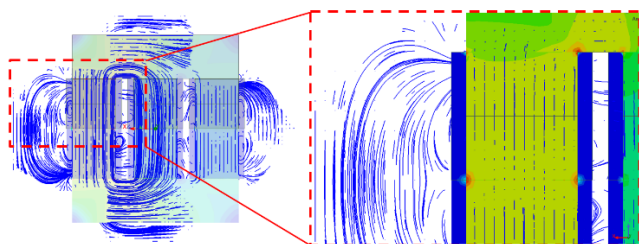
FIGURE 3. Leakage magnetic field of the choke.

to use a geometric approximation [28], [29], [30]. The usual and commonly used approximation elements are reported in [1] and shown in Fig. 4. By comparing Fig. 3 and Fig. 4, we find that the actual magnetic field follows trajectories different from the trajectories prescribed by the descriptive elements, from which arose the need to create completely new approximation elements.

For example, the element Pg assumes a homogeneous magnetic field having parallel flux lines in the whole analyzed volume. In the real situation, the air gap guides the flux lines at different angles and thus increases their overall length.
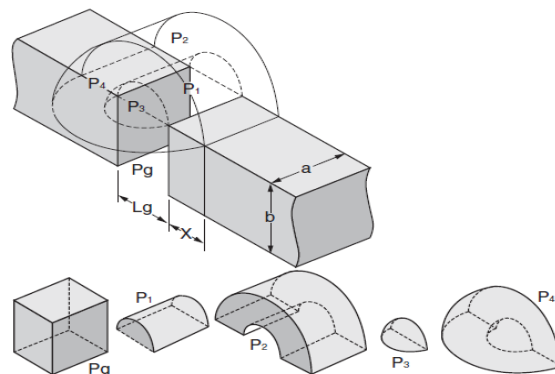
FIGURE 4. Geometric elements describing magnetic flux within inductor air gap.

The flux lines within P1 and P3 arise from a point, i.e., from a geometry with zero cross-section, and form an infinitely large reluctance and thus non-physical results. The situation can be resolved analyzing the geometry combination Pg + P1 + P3 described in Fig. 5, where a quarter of the total volume is assumed.
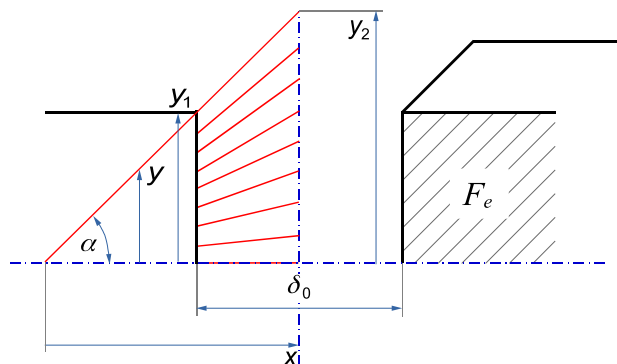
FIGURE 5. Illustrative geometry to derive reluctance of the element Pg+P1+P3.

If the element of the reluctance is given by (12),

$$dR_{m-h} = \frac{dx}{\mu_0 4y^2} \qquad (12)$$

then (13) helps finding (14) as relationship between dx and dy.

$$\tan\alpha = \frac{y}{x} = \frac{y_2 - y_1}{\delta_0/2} \implies x = \frac{\delta_0 y}{2(y_2 - y_1)} \qquad (13)$$

In (14), y_1 and y_2 are integration limits.

$$dx = \frac{\delta_0}{2\,(y_2 - y_1)}dy \tag{14}$$

Substituting (14) back into (12), formula (15) is obtained.

$$
\begin{aligned}
R_{m-h} &= \frac{2}{\mu_0 4}\int_{y_1}^{y_2}\frac{\delta_0}{2\,(y_2 - y_1)\,y^2}dy \\
&= \frac{\delta_0}{\mu_0 4\,(y_2 - y_1)}\int_{y_1}^{y_2}\frac{dy}{y^2} \\
&= \frac{\delta_0}{\mu_0 4 y_1 y_2}
\end{aligned}
\tag{15}
$$

Considering the integration limits, i.e., $y_1 = \frac{a}{2}$, $y_2 = \frac{(a + \delta_0)}{2}$, we find the reluctance as (16).

$$R_{m-h} = \frac{\delta_0}{\mu_0 a\,(a + \delta_0)} \tag{16}$$

Fig. 6 illustrates the descriptive element P2. The element of the permeance is derived from (17).

$$d\lambda_{m-1} = \mu_0\frac{d\vec{S}}{\pi r} \tag{17}$$

Then, (18) is formed from the combination of (17) with Fig. 6.

$$
\begin{aligned}
\lambda_{m-1} &= \mu_0\int_{r_1}^{r_2}\frac{d\vec{S}}{\pi r} = \mu_0\int_{r_1}^{r_2}\frac{a}{\pi r}dr = \mu_0\frac{a}{\pi}\int_{r_1}^{r_2}\frac{dr}{r} \\
&= \mu_0\frac{a}{\pi}ln\left(\frac{r_2}{r_1}\right)
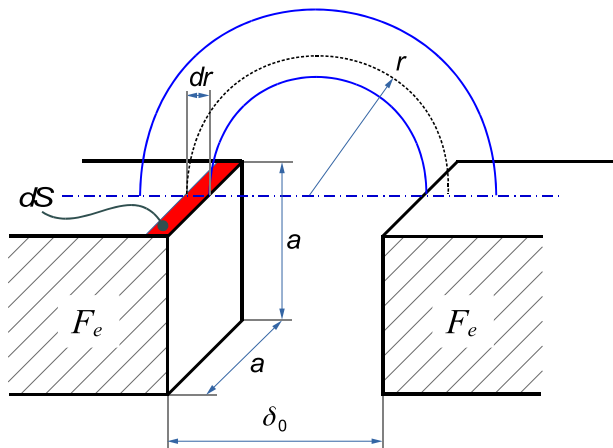\end{aligned}
\tag{18}
$$

FIGURE 6. Illustrative geometry to derive reluctance of the element P2.

Fig. 3 indicates that the P2 elements located in the corners, unlike the other P2 elements, are symmetrical only in the range of 90°. Based on this and (18) we define (19).

$$\lambda_{m-2} = \mu_0\int_{r_1}^{r_2}\frac{d\vec{S}}{\pi/2 r} = \mu_0\int_{r_1}^{r_2}\frac{2a}{\pi r}dr$$

$$
\begin{aligned}
&= \mu_0\frac{2a}{\pi}\int_{r_1}^{r_2}\frac{dr}{r} \\
&= \mu_0\frac{2a}{\pi}ln\left(\frac{r_2}{r_1}\right)
\end{aligned}
\tag{19}
$$

The corresponding reluctances (20) are then defined as the inverse values of (18) and (19).

$$
\begin{aligned}
R_{m-1} &= \frac{1}{\lambda_{m-1}} \\
R_{m-2} &= \frac{1}{\lambda_{m-2}}
\end{aligned}
\tag{20}
$$

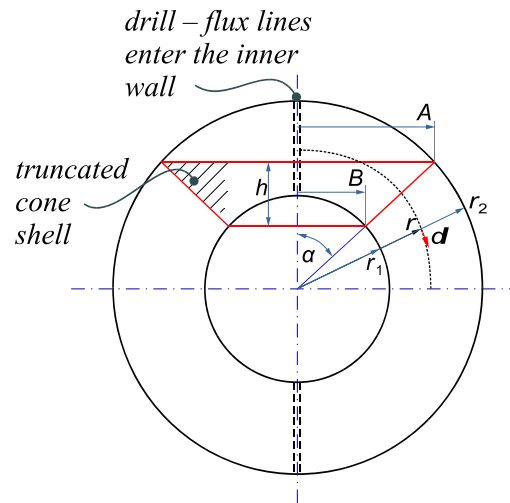Assuming the geometrical situation shown in Fig. 7 we can determine the reluctance of the last element P4.

FIGURE 7. Illustrative geometry to derive reluctance of the element P4.

The analysis is based on the idea of drilled hollow ball and referring (12), we start with writing (21).

$$dR_{m-3} = \frac{dl}{\mu_0 S_k} \tag{21}$$

The correct proceed would be to integrate over the radius r and the angle α, however in this case the length of the flux line equals to its mean value, so we use this fact to simplify the task.

The cross-sectional area through which the flux lines pass has the shape of a truncated cone shell and is given by equation (22).

$$S_k = \pi\,(A + B)\sqrt{h^2 + (A - B)^2} \tag{22}$$

Basic trigonometric manipulation with (22) results in (23).

$$
\begin{aligned}
S_k &= \pi\,(r_1 + r_2)\,sin\alpha\sqrt{[(r_2 - r_1)\,cos\alpha]^2 + [(r_2 - r_1)\,sin\alpha]^2} \\
&= \pi\left(r_2^2 - r_1^2\right)sin\alpha
\end{aligned}
\tag{23}
$$

The actual investigated region has only a quarter area, thus we will integrate the first 90° to get (24).

$$R_{m-3} = \frac{2\frac{r_1+r_2}{2}}{\mu_0 4\pi \left(r_2^2 - r_1^2\right)} \int_0^{\pi/2} \frac{d\alpha}{sin\alpha}$$

$$= \frac{r_1 + r_2}{\mu_0 4\pi \left(r_2^2 - r_1^2\right)} \int_0^{\pi/2} csc\ \alpha d\alpha \qquad (24)$$

The solution of (24) may be find using smart multiplication (25).

$$\int csc\ \alpha \frac{csc\ \alpha + cot\ \alpha}{csc\ \alpha + cot\ \alpha} d\alpha \qquad (25)$$

When the substitution (26) comes in,

$$u = csc\ \alpha + cot\ \alpha$$
$$du = -\left(csc\ \alpha cot\ \alpha + csc^2\alpha\right) d\alpha \qquad (26)$$

relation (27) is obtained.

$$\int csc\ \alpha \frac{csc\ \alpha + cot\ \alpha}{csc\ \alpha + cot\ \alpha} d\alpha = \int \frac{csc^2\alpha + csc\ \alpha\ cot\ \alpha}{csc\ \alpha + cot\ \alpha} d\alpha$$
$$= -\int \frac{du}{u} = -ln\ |u| + c \qquad (27)$$

Combination of (26) and (27) gives (28),

$$\int csc\ \alpha d\alpha = -ln\ |csc\ \alpha + cot\ \alpha| + c \qquad (28)$$

transforming to (29) after the integration limits are considered.

$$R_{m-3} = \frac{r_1 + r_2}{\mu_0 4\pi \left(r_2^2 - r_1^2\right)} \int_0^{\pi/2} csc\ \alpha d\alpha$$

$$= \frac{r_1 + r_2}{\mu_0 4\pi \left(r_2^2 - r_1^2\right)}$$
$$\times \left(ln\ |csc\ 0 + cot\ 0| - ln\ |csc\ ^\pi/_2 + cot\ ^\pi/_2|\right) \qquad (29)$$

As $ln\ |csc\ ^\pi/_2 + cot\ ^\pi/_2| = 0$, (29) can be rewritten into (30).

$$R_{m-3} = \frac{r_1 + r_2}{\mu_0 4\pi \left(r_2^2 - r_1^2\right)} ln\ |csc\ 0 + cot\ 0| \qquad (30)$$

If (30) is investigated more in detail, it is found that this situation represents divergent integral. This situation was expected at the beginning of the analysis, while for this case it is assumed that the flux lines are coming out from the geometry with zero cross-section. The only solution how to solve this issue is to start integration from the values slightly higher than 0. Proposed integration limits are defined as proposed by (31).

$$R_{m-3} = \frac{r_1 + r_2}{\mu_0 4\pi \left(r_2^2 - r_1^2\right)} ln\ |csc\ 0.01 + cot\ 0.01| \qquad (31)$$

B. EQUIVALENT CIRCUIT OF THE MAGNETIC CIRCUIT

For the purposes of magnetic circuit analysis, the standard equivalent schematics (Figure 8) was used together with iteration calculation method [31], [32], [33], [34], [35].
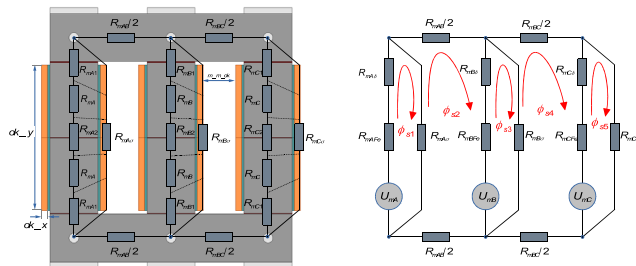

FIGURE 8. Choke reluctances (left) and the resulting equivalent scheme (right).

Identities (32) may be defined from situation shown in Fig. 8.

$$R_{mA\delta} = 2R_{mA1} + R_{mA2}$$
$$R_{mB\delta} = 2R_{mB1} + R_{mB2}$$
$$R_{mC\delta} = 2R_{mC1} + R_{mC2}$$
$$R_{mAFe} = 2R_{mA}$$
$$R_{mBFe} = 2R_{mB}$$
$$R_{mCFe} = 2R_{mC} \qquad (32)$$

Based on conditions (7), one can derive (33).

$$ok\_x = 2r_v + \frac{N - mod(N, k)}{k}\delta$$
$$ok\_y = 2r_v + (k - 1)\delta \qquad (33)$$

The parameter m_m_ok is independent and can therefore be selected. The airgap susceptance's are expressed by (34), where limits in (18) are $r_2 = {ok\_y}/{4} + {\delta_0}/{6}$ and $r_1 = {\delta_0}/{6}$.

$$\lambda_{mA1} = \lambda_{m-h} + 3\lambda_{m-1} + \lambda_{m-2} + 4\lambda_{m-3}$$
$$\lambda_{mA2} = \lambda_{m-h} + 4\lambda_{m-1} + 4\lambda_{m-3}$$
$$\lambda_{mB1} = \lambda_{m-h} + 2\lambda_{m-1} + 2\lambda_{m-2} + 4\lambda_{m-3}$$
$$\lambda_{mB2} = \lambda_{mA2}$$
$$\lambda_{mC1} = \lambda_{mA1}$$
$$\lambda_{mC2} = \lambda_{mA2} \qquad (34)$$

The equivalent circuit includes the leakage fluxes estimated using (18) for which the integration limits are $r_2 = {ok\_y}/{2}$ and $r_1 = {\delta_0}/{6}$. Assuming this (35) is obtained.

$$R_{mA\sigma} = \frac{1}{3\lambda_{mA\sigma}}$$
$$R_{mB\sigma} = \frac{1}{2\lambda_{mA\sigma}}$$
$$R_{mC\sigma} = R_{mA\sigma} \qquad (35)$$

The magnetic core reluctances are then given by (36).

$$R_{mAFe} = \frac{ok\_y - \delta_0 + a}{\mu_A(I)\mu_0 a^2}$$

$$R_{mBFe} = \frac{ok\_y - \delta_0 + a}{\mu_B(I)\mu_0 a^2}$$

$$R_{mCFe} = \frac{ok\_y - \delta_0 + a}{\mu_C(I)\mu_0 a^2}$$

$$R_{mAB} = \frac{2ok\_x + m\_m\_ok + a}{\mu_{AB}(I)\mu_0 a^2}$$

$$R_{mBC} = \frac{2ok\_x + m\_m\_ok + a}{\mu_{BC}(I)\mu_0 a^2} \quad (36)$$

All the necessary quantities have been identified, therefore (37) can be assembled. Here, i denotes the i-th step of the iteration.

$$\left[\boldsymbol{\Phi s_{i+1}}\right] = [\boldsymbol{Rm_i}] \setminus [\boldsymbol{U_m}] \quad (37)$$

Equation (37) represents a recurrent relationship, the solution of which can be found by iterative calculation. It is now beneficial to relabel some parameters

- $R_{mAFe} = R_A$,
- $R_{mAB} = R_{AB}$,
- $R_{mA\delta} = R_{A\delta}$,
- $R_{mA\sigma} = R_{A\sigma}$.

to get more simple equations. Equation (37) is then rewritten as (38), shown at the bottom of the page.

Equation (38) is solved as follows. Initially, the loop magnetic fluxes are obtained from (37), while the core reluctances are set to zero. This gives us the initial approximation for the core flux densities (39) within the i-th computational iteration.

$$B_1 = \frac{\Phi_{s1}}{a^2}$$

$$B_2 = \frac{\Phi_{s2} - \Phi_{s3}}{a^2}$$

$$B_3 = \frac{\Phi_{s4} - \Phi_{s5}}{a^2}$$

$$B_{AB} = \frac{\Phi_{s2}}{a^2}$$

$$B_{BC} = \frac{\Phi_{s4}}{a^2} \quad (39)$$

The actual permeability values are found from BH curve of used magnetic material. The next step is to repeat the calculation (38) until condition (40) is met.

$$\left[\boldsymbol{\Phi s_{i+1}}\right] \approx [\boldsymbol{\Phi s_i}] \quad (40)$$

Core losses can then be determined from the calculated flux densities by any method.

IV. THE PROPOSED METHOD APPLICATION

The previous part of the paper (chapter III.) provides the detailed analysis of the magnetic circuit of the inductor and implementation of the calculation related to the power loss estimation. It is more than useful to provide guideline, which simplifies the procedure of the developed methodology application.

Figure 9 shows algorithm which provides clearer overview about the method, while mathematical formulations from section III are used. Start of the analyses and consequent procedure begin with the selection of the core geometry and core material properties based on standard choke design. From these inputs the proposed method follows by identification of the value of core reluctance considering presence of the airgap within magnetic circuit. After that, the process identifies the magnetic flux densities in the core, starting with zero values of the core reluctances. For each iteration, the permeability value is determined from the magnetic properties (BH curve) of used magnetic material. The computation ends when the condition described by (40) is met.

V. APPLICATION EXAMPLE

Presented methodology is demonstrated on example with parameters as follows.

- $\delta = 1.8 \; mm$
- $r_v = 0.88 \; mm$
- $a = 55 \; mm$
- $\delta_0 = 0.83 \; mm$
- $N = 248 \; mm$
- $I = 10.7 A_{mag}$

The aim is to find the value of k *(numb*er of turns in one layer) at which the coil has the minimal power losses for certain value of current. The magnetic circuit is intentionally analyzed operating over saturated.

A. MODEL DATASETS

Considering selected material properties (M530-50 A) the set of data values of the permeability should be represented using

$$[\boldsymbol{\Phi s_{i+1}}] = \begin{bmatrix} \Phi_{s1i+1} \\ \Phi_{s2i+1} \\ \Phi_{s3i+1} \\ \Phi_{s4i+1} \\ \Phi_{s5i+1} \end{bmatrix}, \quad [\boldsymbol{U_m}] = \begin{bmatrix} I_1 N \\ -I_2 N \\ I_2 N \\ -I_3 N \\ I_3 N \end{bmatrix}$$

$$[\boldsymbol{Rm_i}] = \begin{bmatrix} R_{Ai} + R_{A\delta} + R_{A\sigma} & -R_{A\sigma} & 0 & 0 & 0 \\ -R_{A\sigma} & R_{A\sigma} + R_{ABi} + R_{B\delta} + R_{Bi} & -R_{B\delta} - R_{Bi} & 0 & 0 \\ 0 & -R_{B\delta} - R_{Bi} & R_{Bi+1} + R_{B\delta} + R_{B\sigma} & -R_{B\sigma} & 0 \\ 0 & 0 & -R_{B\sigma} & R_{B\sigma} + R_{BCi} + R_{C\delta} + R_{Ci} & -R_{C\delta} - R_{Ci} \\ 0 & 0 & 0 & -R_{C\delta} - R_{Ci} & R_{Ci} + R_{C\delta} + R_{C\sigma} \end{bmatrix}$$

$$\quad (38)$$

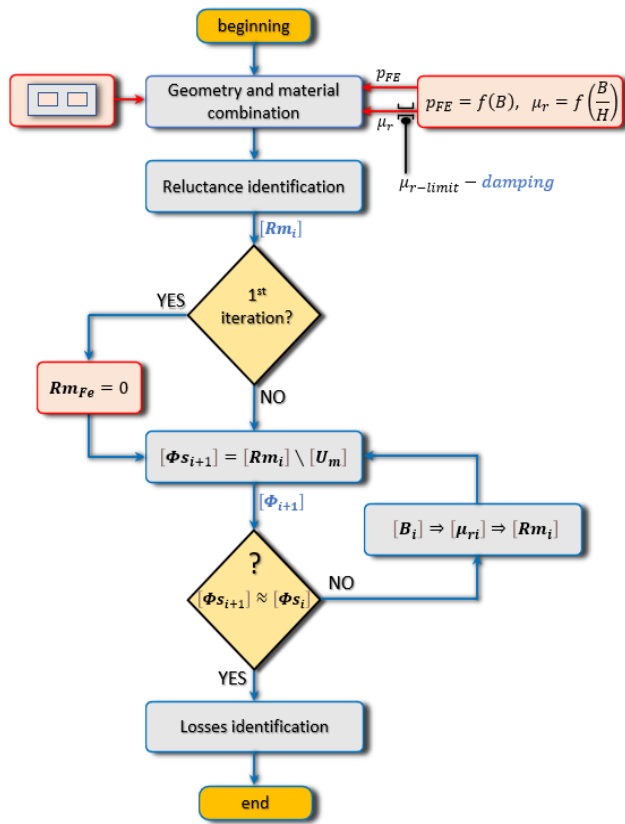**FIGURE 9. Method flowchart description.**

FIGURE 11. Static and dynamic (used by the method) permeability of the material M530-50A.

The specific core losses dependent on the flux density is reported by Fig. 12 and used for iron core losses calculation.

FIGURE 12. Characteristic of the specific losses.

Look-Up-Table function. For this purpose, the BH characteristic will be used (see Figure 10).

FIGURE 10. BH characteristic of the material M530-50A.

Fig. 11 shows the difference between the actual (determined by calculation) and used value of the permeability, while this region is located at $H \geq 10^4$.

In oversaturated states, the mathematical model would oscillate during iteration caused by very low permeabilities, thus convergence may not be achieved. To implement primitive mathematical damping the system permeability constrains must be set.
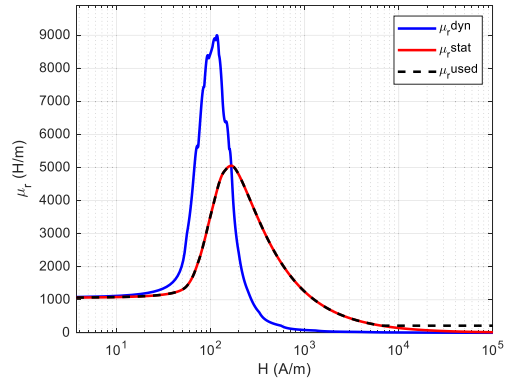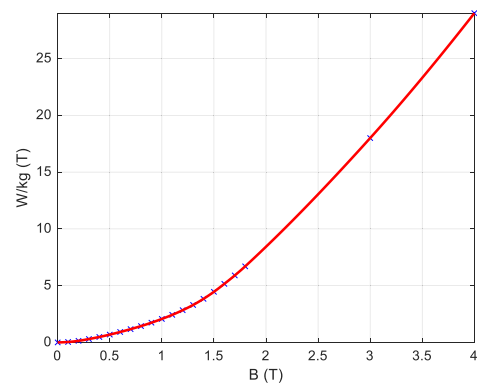
B. RESULTS FOR k = 70
Model convergence is demonstrated on geometry with $k = 70$. For this case, these values are identified:

- $ok\_x = 7.2 \ mm$
- $ok\_y = 126 \ mm$

Substitution into (9) and (11) results in $\Delta P_j = 76.6 \ W$.

Fig. 13 shows the results from the simulation using finite element method. The flux density values are given below, while the arrows (in Fig. 13) identifie the plane under investigation:

- $B_1 = 1.83 \ T$,
- $B_2 = 0.92 \ T$,
- $B_3 = 0.9 \ T$

These results are used for comparison with developed mathematical model. Fig. 14 shows the results of the calculations provided by mathematical model for the situation defined by $k = 70$. We can observe in Fig. 14, that the individual magnetic flux densities reach their values satisfying condition (40) almost after 12 iterations of the computation procedure. This result represents couple of seconds of the calculation performed by a standard office PC.
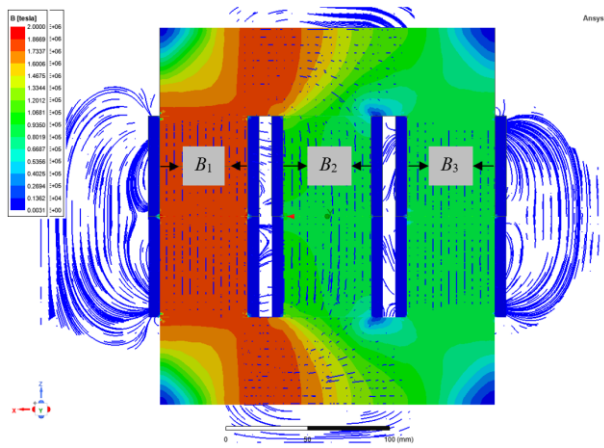
FIGURE 13. Magnetic saturation of the compensation choke (k = 70, m_m_ok = 8 mm).
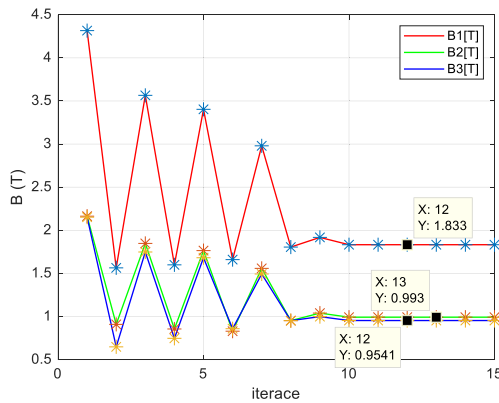

FIGURE 14. Convergence of the proposed mathematical model after 15 iterations.

C. VERIFICATION OF PROPOSED METHODOLOGY BASED ON PARAMETRIC COMPARISON

For the better interpretation, the parametrical verification of the mathematical model is initially given (Table 1). The situation considers the change of the k parameter, while other dimensions and core properties remains the same. The procedure performs parametric calculation changing one independent variable (k in this case) that affects the rest of the choke geometry, while its electromagnetic utilization is preserved. The calculation will determine the volume of the core and the length of the coil for each specified k, and thus the total losses. From this we can very quickly find the minimum losses for the basic electromagnetic design.

Evaluation of the individual power losses was provided, i.e. amount of winding losses (ΔP_W), core losses (ΔP_{FE}), while consequently total losses were estimated using proposed method (ΔP_{tot}). Using FEM analyses and for purposes of comparison, core losses of considered choke have been evaluated (ΔP_{Fe-FEM}).

Results from Table 1 indicate that there is a certain value of k (apparently $k = 50$), for which the total power losses will be minimal. Comparing FEM simulation and mathematical model, a high accuracy is seen for each case.

TABLE 1. The results used for parametrical verification between presented analytical method and fem simulation.

k	ok_x [mm]	ok_y [mm]	ΔP_W [W]	ΔP_{FE} [W]	ΔP_{tot} [W]	ΔP_{FE-FEM} [W]
30	23.4	36	87.1	102.2	189.3	99.9
50	9	90	79	108	187	106.5
70	7.2	126	76.6	121.8	198.4	121.4
90	5.4	162	74.83	136.37	211.2	136.3
110	5.4	198	73.75	153.4	227.15	153.5
			ANALYTICAL MODEL			**FEM**

Simultaneously, another evaluating criterion could be total mass of choke parts (m_{tot}), while both winding mass (m_{cu}) and core mass (m_{Fe}) are evaluated within Table 2.

TABLE 2. Calculation of results reflected to the evaluation of the mass of winding copper material and core material of the compensation choke.

k	ok_x [mm]	ok_y [mm]	m_W [kg]	m_{FE} [kg]	m_{tot} [kg]
30	23.4	36	4.53	15.45	19.98
50	9	90	4.14	16.64	20.78
70	7.2	126	3.99	18.87	22.86
90	5.4	162	3.89	21.1	24.99
110	5.4	198	3.84	23.65	27.49
		ANALYTICAL MODEL			

From the results above, it is possible to understood that even if the core saturation and the current density are fixed, the weight does not necessarily correlate with the total losses. Proof of this is the geometry in the second row (k = 50) of Table 2, where it is possible to identify that even the total mass is higher compared to k = 30, the total power losses are lower (Table 1). Graphical interpretation of data listed in Tab. 1 and Tab. 2. Are presented in Fig. 15.
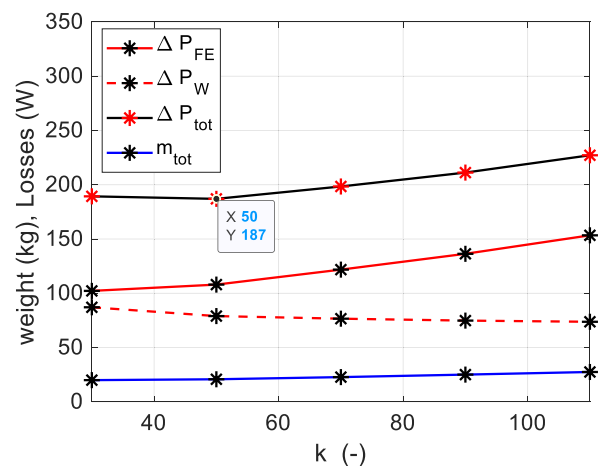

FIGURE 15. Graphical interpretation of data listed in Tab. 1 and Tab. 2.

VI. CONCLUSION

This paper has presented methodology for optimization of the compensation choke design, while the approach is based

on the identification of the fringing flux within the magnetic circuit of the choke. From the achieved results it is seen that magnetic circuit with the airgap was analytically described and approximated following identification of the relationships of the magnetic flux dependencies. Presented approach can be used for any choke design targeting optimization regarding individual power losses of magnetic component (core losses and winding losses). The methodology provides the possibilities to find the solution, which is specific by the lowest total power losses, or the lowest mass of the compensation choke parts. The proposed method was demonstrated using a case study and verified by the finite element analyses (FEA). From the results is seen, that the accuracy of used analytical method for power loss evaluation varied for individual case studies, while relative error was within range from -2.2% (k = 30) $-1,4\%$ (k = 50) $-0,33\%$ (k = 70) up to $-0,05\%$ (k = 110). Based on these achievements, it is worth to deduce that presented methodology represents fast calculating and highly accurate apparatus for the purposes of optimization of compensation choke design. The time required to solve the problem by the analytical method is approximately 156 times shorter as compared to FEA. The comparison was made using a standard office laptop where ANSYS was used for FEA with a calculation time of 1250 seconds and Matlab for the analytical model which reduced the calculation time to 8 seconds.

REFERENCES

[1] I. Laird, X. Yuan, J. Scoltock, and A. J. Forsyth, "A design optimization tool for maximizing the power density of 3-phase DC–AC converters using silicon carbide (SiC) devices," *IEEE Trans. Power Electron.*, vol. 33, no. 4, pp. 2913–2932, Apr. 2018, doi: 10.1109/TPEL.2017.2705805.

[2] S. Ernst, L. Kotulski, T. Lerch, M. Rad, A. Sędziwy, and I. Wojnicki, "Calculating reactive power compensation for large-scale street lighting," in *Computational Science* (Lecture Notes in Computer Science), vol. 12138. Cham, Switzerland: Springer, 2020, doi: 10.1007/978-3-030-50417-5_40.

[3] J. Dixon, L. Moran, J. Rodriguez, and R. Domke, "Reactive power compensation technologies: State-of-the-art review," *Proc. IEEE*, vol. 93, no. 12, pp. 2144–2164, Dec. 2005, doi: 10.1109/JPROC.2005.859937.

[4] H. Tariq, S. Czapp, S. Tariq, K. M. Cheema, A. Hussain, A. H. Milyani, S. Alghamdi, and Z. M. S. Elbarbary, "Comparative analysis of reactive power compensation devices in a real electric substation," *Energies*, vol. 15, no. 12, p. 4453, Jun. 2022, doi: 10.3390/en15124453.

[5] H. Ye, A. Li, and Z. Zhagn, "Overview of reactive power compensation technology based on energy storage," *Energy Storage Sci. Technol.*, vol. 10, no. 6, pp. 2209–2217, 2021.

[6] J. Chysky, J. Novak, and M. Novak, "Losses in sinusoidal filter chokes," in *Proc. 39th Annu. Conf. IEEE Ind. Electron. Soc. (IECON)*, Nov. 2013, pp. 7790–7794, doi: 10.1109/IECON.2013.6700433.

[7] D. K. Saini, A. Ayachit, A. Reatti, and M. K. Kazimierczuk, "Analysis and design of choke inductors for switched-mode power inverters," *IEEE Trans. Ind. Electron.*, vol. 65, no. 3, pp. 2234–2244, Mar. 2018, doi: 10.1109/TIE.2017.2740847.

[8] F. Bachheibl and D. Gerling, "Iron loss estimation for highly distorted currents in inverter output chokes," in *Proc. IEEE Int. Electric Mach. Drives Conf. (IEMDC)*, May 2015, pp. 1260–1264, doi: 10.1109/IEMDC.2015.7409223.

[9] Y. Liu, K. Y. See, and R. Simanjorang, "3-D modeling of common mode choke for thermal analysis," in *Proc. Asia–Pacific Int. Symp. Electromagn. Compat. (APEMC)*, Jun. 2017, pp. 79–81, doi: 10.1109/APEMC.2017.7975430.

[10] V. C. Valchev, T. P. Todorova, P. V. Yankov, and A. Van den Bossche, "Design considerations and loss analysis of DC chokes," in *Proc. 19th Int. Symp. Electr. App. Technol. (SIELA)*, May 2016, pp. 1–3, doi: 10.1109/SIELA.2016.7543062.

[11] A. Fatemi, D. M. Ionel, N. A. O. Demerdash, D. A. Staton, R. Wrobel, and Y. C. Chong, "Computationally efficient strand eddy current loss calculation in electric machines," *IEEE Trans. Ind. Appl.*, vol. 55, no. 4, pp. 3479–3489, Jul. 2019, doi: 10.1109/TIA.2019.2903406.

[12] E. Ramirez-Laboreo, M. G. L. Roes, and C. Sagues, "Hybrid dynamical model for reluctance actuators including saturation, hysteresis, and eddy currents," *IEEE/ASME Trans. Mechatronics*, vol. 24, no. 3, pp. 1396–1406, Jun. 2019, doi: 10.1109/TMECH.2019.2906755.

[13] A. Tessarolo, "Analytical determination of slot leakage field and inductances of electric machines with double-layer windings and semiclosed slots," *IEEE Trans. Energy Convers.*, vol. 30, no. 4, pp. 1528–1536, Dec. 2015, doi: 10.1109/TEC.2015.2458181.

[14] S. De Caro, S. Foti, T. Scimone, A. Testa, M. Cacciato, G. Scarcella, and G. Scelba, "THD and efficiency improvement in multi-level inverters through an open end winding configuration," in *Proc. IEEE Energy Convers. Congr. Exposit. (ECCE)*, Sep. 2016, pp. 1–7, doi: 10.1109/ECCE.2016.7855496.

[15] M. Damnjanovic, L. Zivanov, and G. Stojanovic, "Analysis of effects of material and geometrical characteristics on the performance of SMD common mode choke," in *Proc. 26th Int. Conf. Microelectron.*, May 2008, pp. 267–270, doi: 10.1109/ICMEL.2008.4559271.

[16] Y. Li, J. Du, Y. Jing, and D. Zou, "Simulated analysis and experimental study of winding leakage magnetic field in short circuit of three-phase three-column dry-type transformer," in *Proc. IEEE Int. Conf. Appl. Supercond. Electromagn. Devices (ASEMD)*, Oct. 2020, pp. 1–2, doi: 10.1109/ASEMD49065.2020.9276272.

[17] K. Fujisaki, M. Fujikura, J. Mino, and S. Satou, "Three-dimensional magnetic field numerical calculation by equivalent $B - -H$ method for magnetic field mitigation," *IEEE Trans. Magn.*, vol. 46, no. 5, pp. 1147–1154, May 2010, doi: 10.1109/TMAG.2009.2039939.

[18] H. Wu and B. Bai, "Calculation of magnetic flux leakage and temperature field in new power transformer," in *Proc. IEEE Magn. Conf. (INTERMAG)*, May 2015, p. 1, doi: 10.1109/INTMAG.2015.7157212.

[19] H. B. Ertan, K. Leblebicioglu, B. Avenoglu, and B. Ercan, "Identification of parameters of an induction motor from field solution," in *Proc. 6th Int. Conf. Elect. Mach. Syst.*, Nov. 2003, pp. 1–6.

[20] N. Zhu, J. Kang, D. Xu, B. Wu, and Y. Xiao, "An integrated AC choke design for common-mode current suppression in neutral-connected power converter systems," *IEEE Trans. Power Electron.*, vol. 27, no. 3, pp. 1228–1236, Mar. 2012, doi: 10.1109/TPEL.2011.2162748.

[21] M. Kaltenbacher, *Numerical Simulation of Mechatronic Sensors and Actuators*. 2nd ed. Berlin, Germany: Springer, 2007.

[22] W. Rohouma, R. S. Balog, A. A. Peerzada, and M. M. Begovic, "Reactive power compensation of time-varying load using capacitor-less D-STATCOM," in *Proc. 10th Int. Conf. Power Electron. ECCE Asia (ICPE-ECCE Asia)*, May 2019, pp. 2296–2301, doi: 10.23919/ICPE2019-ECCEAsia42246.2019.8796869.

[23] A. Testa, S. De Caro, A. Consoli, and M. Cacciato, "An active current ripple compensation technique in grid connected fuel cell applications," in *Proc. IEEE Energy Convers. Congr. Expo.*, Sep. 2009, pp. 2642–2649, doi: 10.1109/ECCE.2009.5316104.

[24] D. Neumayr, D. Bortis, J. W. Kolar, S. Hoffmann, and E. Hoene, "Origin and quantification of increased core loss in MnZn ferrite plates of a multi-gap inductor," *CPSS Trans. Power Electron. Appl.*, vol. 4, no. 1, pp. 72–93, Mar. 2019, doi: 10.24295/CPSSTPEA.2019.00008.

[25] B. Liu, W. Chen, J. Wang, and Q. Chen, "A practical inductor loss testing scheme and device with high frequency pulsewidth modulation excitations," *IEEE Trans. Ind. Electron.*, vol. 68, no. 5, pp. 4457–4467, May 2021, doi: 10.1109/TIE.2020.2984985.

[26] T. Shimizu, K. Kakazu, K. Takano, and H. Ishii, "Loss evaluation of AC filter inductor core on a PWM converter," in *Proc. 8th Int. Conf. Power Electron. (ECCE Asia)*, May 2011, pp. 1047–1052, doi: 10.1109/ICPE.2011.5944704.

[27] P. Y. Huang and T. Shimizu, "High power/current inductor loss measurement with shunt resistor current-sensing method," in *Proc. Int. Power Electron. Conf. (IPEC-Niigata-ECCE Asia)*, May 2018, pp. 2165–2169, doi: 10.23919/IPEC.2018.8507755.

[28] A. Tessarolo, S. Mohamadian, and M. Bortolozzi, "A new method for determining the leakage inductances of a nine-phase synchronous machine from no-load and short-circuit tests," *IEEE Trans. Energy Convers.*, vol. 30, no. 4, pp. 1515–1527, Dec. 2015, doi: 10.1109/TEC.2015.2458182.

[29] A. H. Fathi, S. Hoseinnia, and R. Roshandel, "A novel isolated DC/DC converter for fuel cell powered load," in *Proc. IEEE Electr. Power Energy Conf. (EPEC)*, Oct. 2009, pp. 1–6, doi: 10.1109/EPEC.2009.5420987.

[30] T. Sato, S. Aya, H. Igarashi, M. Suzuki, Y. Iwasaki, and K. Kawano, "Loss computation of soft magnetic composite inductors based on interpolated scalar magnetic property," *IEEE Trans. Magn.*, vol. 51, no. 3, pp. 1–4, Mar. 2015, doi: 10.1109/TMAG.2014.2359983.

[31] W. Wang, S. de Haan, J. A. Ferreira, and F. Pansier, "A novel and simple method to distinguish winding loss from inductor loss under practical excitations," in *Proc. 39th Annu. Conf. IEEE Ind. Electron. Soc. (IECON)*, Nov. 2013, pp. 252–257, doi: 10.1109/IECON.2013.6699144.

[32] M. Galad, P. Spanik, M. Cacciato, and G. Nobile, "Comparison of common and combined state of charge estimation methods for VRLA batteries," in *Proc. ELEKTRO*, May 2016, pp. 220–225, doi: 10.1109/ELEKTRO.2016.7512069.

[33] J. Wang, K. J. Dagan, X. Yuan, W. Wang, and P. H. Mellor, "A practical approach for core loss estimation of a high-current gapped inductor in PWM converters with a user-friendly loss map," *IEEE Trans. Power Electron.*, vol. 34, no. 6, pp. 5697–5710, Jun. 2019, doi: 10.1109/TPEL.2018.2867264.

[34] S. F. Roberto, D. Scire, G. Lullo, and G. Vitale, "Equivalent circuit modelling of ferrite inductors losses," in *Proc. IEEE 4th Int. Forum Res. Technol. Soc. Ind. (RTSI)*, Sep. 2018, pp. 1–4, doi: 10.1109/RTSI.2018.8548450.

[35] Y.-S. Quan and J. Shan, "Mechanical forces and magnetic field simulation of transformer with finite element method," in *Proc. 2nd Int. Conf. Mechanic Automat. Control Eng.*, Jul. 2011, pp. 1390–1393, doi: 10.1109/MACE.2011.5987204.

BOHUMIL SKALA was born in Pilsen, Czech Republic, in 1973. He received the master's (Ing.), Ph.D., and Doc. degrees in electrical engineering from the University of West Bohemia, Pilsen, Czech Republic, in 1996, 2001, and 2006, respectively.

From 1996 to 2006, he was an Assistant with the Electrical Machines Laboratory. Since 2006, he has been an Assistant Professor with the Electrical Engineering Department and the Chief of the Laboratory of Electrical Machines. He is the author of more than ten books, more than 150 articles, and more than 70 inventions. He holds two patents. His research interests include design of transformers and rotary electrical machines, winding design of the synchronous generator, and tests and measurements on electrical machines.

VLADIMIR KINDL (Member, IEEE) received the Ph.D. degree in electrical engineering from the University of West Bohemia, Czech Republic, in 2011.

He was appointed as a Lecturer in electric machines. In the same year, he joined the Regional Innovation Centre for Electrical Engineering—RICE, where he works as a Research and Development Engineer. His main research interests include power electronics—wireless power transfer, electric machines, and finite element simulations.

MICHAL FRIVALDSKY (Member, IEEE) was born in Stara Lubovna, Slovakia, in 1983. He received the master's (Ing.) degree, in 2006, and the Ph.D. degree from the Faculty of Electrical Engineering, University of Žilina (FEE-UNIZA), in 2009. After study, his working activities have been associated to a Researcher and an Assistant Professor within power electronics and power converter systems at the Department of Mechatronics and Electronics, FEE-UNIZA, where he received the Associate Professor Degree, in 2013. Since 2017, he has been working as the Head of the Department of Mechatronics and Electronics, FEE-UNIZA, and he gained the tittle of a Professor, in 2021. He is the author of more than 130 articles, more than 20 inventions, and five books. His research interests include power electronic systems, switched mode power supplies, resonant converters, power semiconductor devices, wireless power transfer, power density, efficiency optimization, thermal management, thermal modeling, lifetime optimization, e-mobility, alternative transport systems, and modern concepts of power electronic systems for intelligent grids.

• • •